Available online at www.sciencedirect.com
SCIENCE DIRECT®
Electrochimica Acta 50 (2005) 3407–3413
ELECTROCHIMICA Acta
www.elsevier.com/locate/electacta

Crystallographic and electrochemical characteristics of $La_{0.7}Mg_{0.3}Ni_{3-x}(Al_{0.5}Mo_{0.5})_x$ (x = 0–0.4) hydrogen storage alloys

X.B. Zhang[a], D.Z. Sun[b], W.Y. Yin[a], Y.J. Chai[a], M.S. Zhao[a,*]

[a] *Key Laboratory of Rare Earth Chemistry and Physics, Changchun Institute of Applied Chemistry, Chinese Academy of Sciences, Graduate School of Chinese Academy of Sciences, Changchun 130022, PR China*
[b] *State Key Laboratory of Electro-analytical Chemistry, Changchun Institute of Applied Chemistry, Chinese Academy of Sciences, Graduate School of Chinese Academy of Sciences, Changchun 130022, PR China*

Received 16 November 2004; received in revised form 13 December 2004; accepted 18 December 2004
Available online 9 February 2005

Abstract

The effect of partial substitution of Al and Mo for Ni on the structure and electrochemical properties of the $La_{0.7}Mg_{0.3}Ni_{3-x}(Al_{0.5}Mo_{0.5})_x$ (x = 0–0.4) hydrogen storage alloys have been investigated systematically. The result of X-ray powder diffraction (XRD) and Rietveld analysis show that all the alloys consist of the La(La, Mg)$_2$Ni$_9$ phase and the $LaNi_5$ phase. Meanwhile, the lattice parameter and the cell volume of both the La(La, Mg)$_2$Ni$_9$ phase and the $LaNi_5$ phase increase with increasing Al and Mo contents in the alloys. The pressure composition isotherms curves indicate that the hydrogen storage capacity first increases and then decreases with increasing x. The electrochemical measurements show that the maximum discharge capacity of the alloy electrodes first increases from 343.3 (x = 0) to 377.6 mAh/g (x = 0.3) and then decreases to 350.4 mAh/g (x = 0.4). Moreover, the high rate dischargeability (HRD) and the exchange current density of the alloy electrodes decrease first and then increases with the increase of x in the alloys. The hydrogen diffusion coefficient increases with increasing Al and Mo content and thus increases the low temperature dischargeability (LTD) of the alloy electrodes.

Keywords: Hydrogen storage alloy; Metal hydride electrode; Crystal structure; Electrochemical properties

1. Introduction

Hydrogen is expected to be a promising new energy source to replace conventional fossil for solving shortage of fossil energy resources and global warming in near future. In order for hydrogen to become a viable solution to the energy crisis and the environmental problem the hydrogen storage is one of many important processes. Among different ways to store hydrogen, absorption in solid to form hydride is very attractive since it allows safe storage at pressure and temperature close to ambient conditions [1]. It is the most successful for the metal hydrides to be applied as a negative electrode material in many application fields of metal hydrides. Nickel metal hydride (Ni-MH) secondary battery has been widely adopted in various portable electronic devices, electric hand tools and hybrid electric vehicles [2–6]. To date, almost all commercial Ni-MH batteries are employing AB_5-type alloys as the negative electrode materials [7]. However, the electrochemical capacity of the AB_5-type alloys is limited by the single $CaCu_5$-type hexagonal structure [8], the energy densities of the Ni-MH batteries are not competing favorably with some other advanced secondary batteries. Therefore, it is necessary to search for new type alloys with much high energy density, better rate dischargeability and lower cost, which perhaps may be alternative for the conventional rare earth-based AB_5-type alloys or another choice [9].

Recently, R–Mg–Ni (R = rare earth element, Ca or Y) system hydrogen storage electrode for Ni-MH batteries have attracted considerable attention because of their higher hydrogen storage capacities (absorb–desorb 1.8–1.87 wt.% H_2) than of the $LaNi_5$ alloy (absorb–desorb 1.4 wt.% H_2)

* Corresponding author. Tel.: +86 431 5262365; fax: +86 431 5685653.
E-mail address: zhaoms@ciac.jl.cn (M.S. Zhao).

0013-4686/$ – see front matter © 2004 Elsevier Ltd. All rights reserved.
doi:10.1016/j.electacta.2004.12.020

[10–14]. As to their electrochemical hydrogen storage, Chen et al. [6] found that the maximum discharge capacity of $LaCaMgNi_9$ alloy reached 356 mAh/g. Kohno et al. [15] have studied the structure and electrochemical characteristics of La–Mg–$(NiCo)_x$ ($x = 3$–3.5) system alloys and found that $La_{0.7}Mg_{0.3}Ni_{2.8}Co_{0.5}$ alloy reached 410 mAh/g. Although the La–Mg–Ni–Co alloy has high hydrogen storage capacity, the cyclic stability is too low to be used as negative material of the Ni-MH secondary batteries [16], and hence their cycling stability has to be upgraded for practical applications. In commercial AB_5-type alloys the presence of 10 wt.% of Co has indeed improved the cycling life of Ni-MH batteries. However, it influences negatively the discharge capacity as well as initial activation and it constitutes about 40% of the material cost [17]. Much effort has been devoted to search for cheaper substitute element with high reliability to improve the cycling life of Ni-MH batteries. It is believed that Al is one of the best candidates for cobalt substitution [18]. However, Al addition is detrimental to hydrogen diffusion from electrode surface to alloy bulk and thus inevitably decrease the high rate dischargeability (HRD) of alloy electrode [19]. It is reported that Mo addition can remarkably increase the kinetic property [20] as well as the electrochemical capacity of alloy electrode [21]. Therefore, it can be expected that the overall electrochemical properties of the La–Mg–Ni type hydrogen storage alloys could be improved by substitution of Al and Mo for Ni in the alloys.

In present study, the structure and electrochemical characteristics of the $La_{0.7}Mg_{0.3}Ni_{3-x}(Al_{0.5}Mo_{0.5})_x$ ($x = 0$–0.4) hydrogen storage alloys has been investigated systematically.

2. Experimental details

2.1. Alloy preparation and X-ray diffraction analysis

All alloys were prepared by arc-melting carefully the constituent elements with the purity all above 99.9% on a water-cooled copper hearth under argon atmosphere. A slight excess of Mg over composition was needed to compensate for evaporative loss of Mg under preparation conditions. The alloys were turned over and remelted five times to ensure the good homogeneity. The weight loss of the alloys is less than 1 mass% during melting. Therefore, no chemical analyses were carried out. Thereafter, the alloy samples were crushed in mortar into fine powders of -300 meshes powder.

Crystallographic characteristics of the hydrogen storage alloys were investigated by X-ray diffraction on Rigaku D/Max 2500PC X-ray diffractometer (Cu Kα radiation, Bragg-Brentano geometry, 2θ range 10–100°, step size 0.02°, 4 s per step, backscattered rear graphite monochromator). The lattice constants and cell volume were calculated by Rietica program [22]. Silicon is used as standard reference material to calibrate the instrument before we obtain the XRD data.

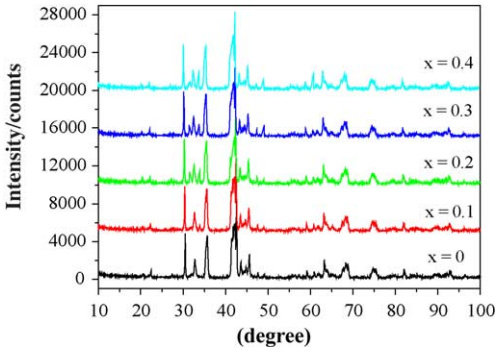

Fig. 1. XRD patterns of the $La_{0.7}Mg_{0.3}Ni_{3-x}(Al_{0.5}Mo_{0.5})_x$ hydrogen storage alloy.

2.2. Electrochemical measurement

The preparation of the disk-type electrodes, the set-up of the electrochemical cell and the measurement of electrochemical properties were similar as described in our previous paper [23]. Pressure–composition isotherms (P–C–T) curves, HRD, linear polarization curves and coefficient of diffusion of the alloy electrodes were measured according to our previous paper [24].

3. Results and discussion

3.1. Crystal structure

The X-ray diffraction patterns of the $La_{0.7}Mg_{0.3}Ni_{3-x}(Al_{0.5}Mo_{0.5})_x$ ($x = 0$–0.4) hydrogen storage alloys are shown in Fig. 1. It can be seen that all alloys have similar diffraction patterns, which indicates that the structure of the alloys almost unchanged with increasing Al and Mo content in the alloys. Moreover, careful examination of the diffraction angle reveals that the diffraction peaks shift to lower angles as a function of the increase of Al and Mo content in the alloys. Fig. 2 shows the XRD pattern and Rietveld analysis pattern of the $La_{0.7}Mg_{0.3}Ni_{2.9}(Al_{0.5}Mo_{0.5})_{0.1}$ hydrogen storage alloy as a representative example of $La_{0.7}Mg_{0.3}Ni_{3-x}(Al_{0.5}Mo_{0.5})_x$

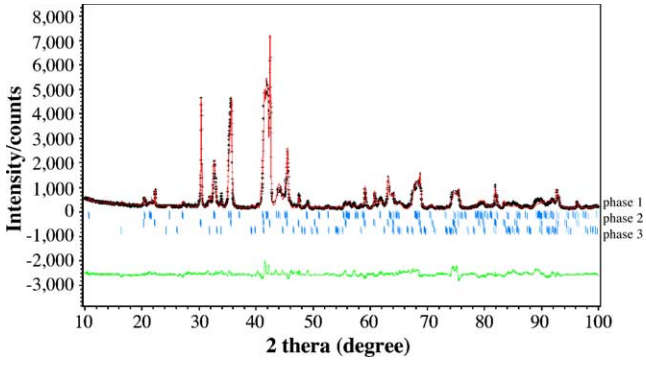

Fig. 2. Rietveld refinement pattern of the XRD profiles for the $La_{0.7}Mg_{0.3}Ni_{2.9}$ $(Al_{0.5}Mo_{0.5})_{0.1}$ hydrogen storage alloy (phase 1: La (La, $Mg)_2Ni_9$; phase 2: $LaNi_5$; phase 3: LaNi).

Table 1
Crystallographic parameters for La_2MgNi_9 by using X-ray diffraction Cu $K\alpha_1$ ($\lambda = 1.5405981$ Å) at 298 K in a space group *R*-3*m* and *Z* = 3[a]

Atom	Site	Metal atom position			Occupancy
		x	*y*	*z*	
La1	3a	0	0	0	1
La2	6c	0	0	0.14669 (11)	0.487
Mg1	6c	0	0	0.14669 (11)	0.513
Ni1	6c	0	0	0.3281 (7)	1
Ni2	3b	0	0	0.5	1
Ni3	18h	0.4987 (3)	0.4988 (6)	0.08327 (16)	1

[a] Structure was refined by using the Rietveld refinement program Rietica. The pattern factor $R_p = 6.7$, the weighted pattern factor $R_{wp} = 9.0$ and the goodness of fit $S = 2.5$.

(x = 0–0.4) hydrogen storage alloys. It can be seen that the calculated pattern by Rietveld method is in good agreement with the observed patterns. Besides small amount of LaNi phase, all alloys consist of a La_2MgNi_9 phase with a $PuNi_3$-type rhombohedral structure and a $LaNi_5$ phase with a $CaCu_5$-type hexagonal structure. The final Rietveld structure parameter of the La_2MgNi_9 phase is tabulated in Table 1. The crystallographic results reveal that La atoms in La_2MgNi_9 can locate both at the 3a site and at the 6c site, while Mg atoms can only locate the 6c site, indicating that the alloy is a ordered compound with the same structure as the previously reported RMg_2Ni_9 (R = La, Ca, Y) alloys. So the final forum of La_2MgNi_9 phase can be designated as $La(La, Mg)_2Ni_9$. The lattice parameter, cell volume, and phase abundance of various phases of the hydrogen storage alloys are listed in Table 2. Variations of the cell parameters and volumes as a function of x in the alloys are shown in Fig. 3. It can be seen that a and c parameters of both the $La(La, Mg)_2Ni_9$ phase and the $LaNi_5$ phase in the alloys increase linearly with the increase of x, which is mainly ascribed to the fact that the atomic radius of Al (1.432 Å) and Mo (1.363 Å) is larger than

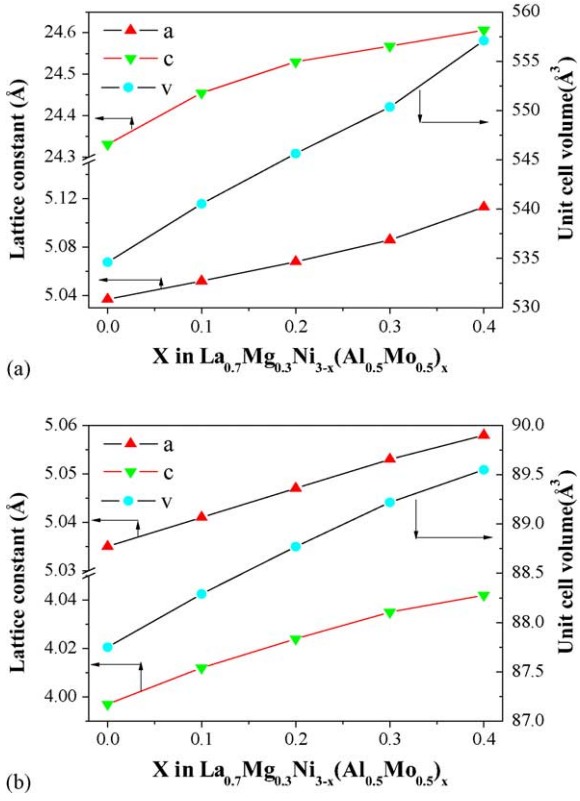

Fig. 3. Variations of the cell parameters and volumes as the function of x in $La_{0.7}Mg_{0.3}Ni_{3-x}$ $(Al_{0.5}Mo_{0.5})_x$ hydrogen storage alloys (x = 0–0.4).

that of Ni (1.246 Å). The Fig. 4 shows the abundances of the $La(La, Mg)_2Ni_9$ phase and the $LaNi_5$ phase as a function of x in the alloys. It can be seen that the $La(La, Mg)_2Ni_9$ phase abundance decrease from 79.56% to 60.16% with increasing of x, however the $LaNi_5$ phase abundance increases from 16.64% to 30.64%. These results will influence the hydro-

Table 2
Characteristics of alloy phases in $La_{0.7}Mg_{0.3}Ni_{3-x}(Al_{0.5}Mo_{0.5})_x$ (x = 0–0.4) alloys [a]

Sample	Phase	Phase abundance (wt.%)	Lattice parameter (Å)			Cell volume (Å)
			a	*b*	*c*	
$x = 0.0$	$La(La, Mg)_2Ni_9$	79.56	5.037	5.037	24.331	534.61
	$LaNi_5$	16.64	5.035	5.035	3.997	87.75
	LaNi	3.8	3.821	11.002	4.454	187.24
$x = 0.1$	$La(La, Mg)_2Ni_9$	74.82	5.052	5.052	24.455	540.54
	$LaNi_5$	20.68	5.041	5.041	4.012	88.29
	LaNi	4.5	3.823	11.004	4.457	187.5
$x = 0.2$	$La(La, Mg)_2Ni_9$	69.98	5.068	5.068	24.530	545.63
	$LaNi_5$	23.62	5.047	5.047	4.024	88.77
	LaNi	6.4	3.827	11.009	4.459	187.86
$x = 0.3$	$La(La, Mg)_2Ni_9$	66.77	5.086	5.086	24.568	550.37
	$LaNi_5$	25.43	5.053	5.053	4.035	89.22
	LaNi	7.8	3.831	11.013	4.461	188.21
$x = 0.4$	$La(La, Mg)_2Ni_9$	60.16	5.113	5.113	24.606	557.09
	$LaNi_5$	30.64	5.058	5.058	4.042	89.55
	LaNi	9.2	3.836	11.021	4.464	188.72

[a] The Rietveld refinement program RIETICA was used.

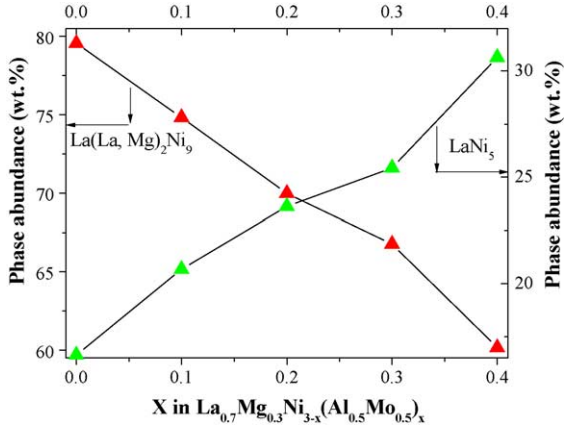

Fig. 4. Phase abundance of the La(La, Mg)$_2$Ni$_9$ phase and the LaNi$_5$ phase existing in the $La_{0.7}Mg_{0.3}Ni_{3-x}(Al_{0.5}Mo_{0.5})_x$ (x = 0–0.4) alloys.

gen storage and electrochemical characteristics of the alloys studied.

3.2. P–C isotherms

Fig. 5 shows the hydrogen desorption electrochemical pressure–composition isotherms (P–C–T) of the $La_{0.7}Mg_{0.3}Ni_{3-x}(Al_{0.5}Mo_{0.5})_x$ (x = 0, 0.1, 0.2, 0.3, 0.4) alloy electrodes at 298 K. It can be seen that the desorption pressure reduces continually as the Al and Mo additions increase. This means that the stability of the hydrides of alloys increases with the increasing Al and Mo content in the alloys. This is because of the unit cell volume of the alloys increases with increasing Al and Mo additions in the alloys. Moreover, Oesterreicher et al. pointed out that the unit cell of the AB_3 compounds contains one-third AB_5 structure and two-thirds AB_2 structure [10]. Therefore, we can assume that the plateau pressure of the La(La, Mg)$_2$Ni$_9$ phase is similar to that of the LaNi$_5$ phase or the difference between their plateau pressures of AB_3 and AB_5 compounds is too small to be observed. The plateau characteristic of the P–C–T curve shown in Fig. 5 gives evidence of our supposition. With the increase of Al and Mo content in the alloy, the hydrogen storage capacity increases from 0.899 to 0.991. This is mainly attributed to the decrease in plateau pressure which enhances the intrinsic hydrogen storage capacity of alloys. However, when x further increase to 0.4, the hydrogen storage capacity decreases to 0.921, which can be attributed to the change in the relative amounts of La(La, Mg)$_2$Ni$_9$ phase and LaNi$_5$ phase owing to Al and Mo substitution. According to the work of Oesterreicher et al. [25], the hydrogen storage capacity of the LaNi$_3$ phase is larger than that of the LaNi$_5$ phase. Therefore, with the decrease of the La(La, Mg)$_2$Ni$_9$ phase in the alloys, the hydrogen storage capacity would decrease accordingly.

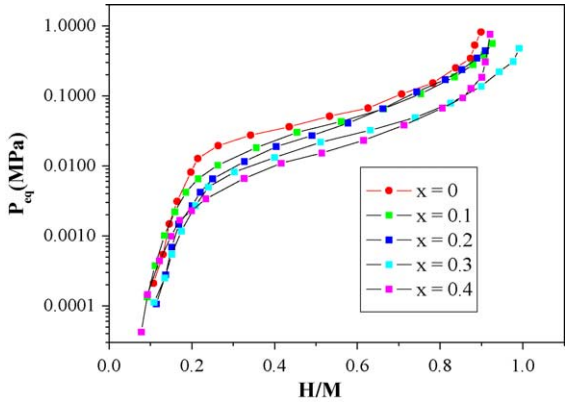

Fig. 5. The electrochemical desorption P–C–T curves for $La_{0.7}Mg_{0.3}Ni_{3-x}(Al_{0.5}Mo_{0.5})_x$ (x = 0, 0.1, 0.2, 0.3, 0.4) alloys at 298 K.

Table 3
Summary of the electrode performance of $La_{0.7}Mg_{0.3}Ni_{3-x}(Al_{0.5}Mo_{0.5})_x$ (x = 0–0.4) alloy electrodes

Samples	H/M	C_{max} (mAh/g)	N_a[a]	HRD$_{1200}$[b] (%)	S_{70} (%)
x = 0.0	0.899	343.3	2	61.3	49.3
x = 0.1	0.926	353.5	3	59.2	55.7
x = 0.2	0.944	359.8	3	69.8	60.5
x = 0.3	0.991	377.6	2	77.6	64.4
x = 0.4	0.921	350.4	2	81.2	68.8

[a] The cycle numbers needed to activate the electrodes.
[b] The high rate dischargeability at the discharge current density of 1200 mA/g.

3.3. Discharge capacity and discharge potential

The cycle numbers needed for activation and maximum discharge capacity of the $La_{0.7}Mg_{0.3}Ni_{3-x}(Al_{0.5}Mo_{0.5})_x$ (x = 0, 0.1, 0.2, 0.3, 0.4) alloy electrodes are listed in Table 3. It can be seen that all these alloys can be easily activated to reach the maximum capacity within three cycles, which means that activation of La–Mg–Ni–Al–Mo alloy electrodes is easy. The maximum discharge capacities of the alloy electrodes first increases from 343.3 mAh/g (x = 0) to 377.6 mAh/g (x = 0.3) and then decreases to 350.4 mAh/g (x = 0.4) when Al and Mo content increases from 0 to 0.4, which is basically consistent with the results of the P–C–T measurement mentioned above. Fig. 6 shows the discharge curves of the 4th

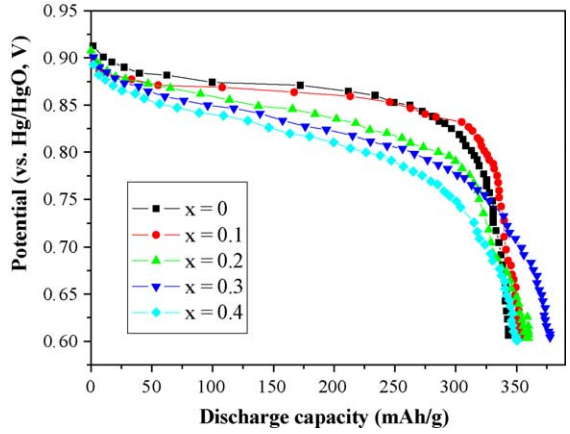

Fig. 6. The discharge curves of $La_{0.7}Mg_{0.3}Ni_{3-x}(Al_{0.5}Mo_{0.5})_x$ (x = 0–0.4) alloy electrodes at the discharge current density of 60 mA/g and 298 K.

cycle for the alloy electrodes at 60 mA/g and 298 K. It can be easily seen that each curve has a wide discharge potential plateau based on the oxidation of desorbed hydrogen from the hydride. It should be noted that the discharge plateau shifts towards a more positive potential as Al and Mo additions increase in the alloys, indicating that the partial substitution of Al and Mo leads to an increase in discharge overpotential of the alloy electrode at different extent.

3.4. Cyclic stability

The cyclic capacity retention rate after 70 cycles at 60 mA/g, expressed as S_{70} (%) = $C_{70}/C_{max} \times 100$ (where C_{max} is the maximum discharge capacity, C_{70} is the discharge capacity at the 70th cycles), is also listed in Table 3. It can be seen that the S_{70} of the alloy electrodes increases noticeably from 49.3% to 68.8% with x increasing from 0 to 0.4, indicating that the cyclic stability of the La–Mg–Ni system alloys is improved markedly along with the increase of Al and Mo content in the alloys. As reported previously [2,5], the formation of passive layer of $La(OH)_3$ and Mg $(OH)_2$ on the alloy surface is ascribed as the main cause of cycling capacity degradation, because such a layer decreases the content of hydrogen absorption elements La and Mg in the alloys and thus reduces hydrogen storage capacity of the alloy. It is known that Al substitution results in the formation of protective oxide (hydroxide) of Al on the alloy surface and a subsequent strong protection to the alloy from further corrosion of La and Mg [26,27]; therefore results in an obviously increase of cycling capacity retention rate of the alloy electrodes. Further investigations in this aspect are going on in our research group.

3.5. High rate dischargeability and electrochemical kinetics

It is very important to restrain the decrease of the discharge capacity even at the high charge/discharge current density. Fig. 7 shows the relationship between the high rate dischargeability and discharge current density of the $La_{0.7}Mg_{0.3}Ni_{3-x}(Al_{0.5}Mo_{0.5})_x$ (x = 0–0.4) alloy electrodes. To make the comparison more exact, the HRD of the alloy electrodes for the discharge current density of 1200 mA/g are also listed in Table 3. It can be seen that as the x increases, the HRD of the alloy electrodes decreases first from 61.3% (x = 0) to 59.2% (x = 0.1), and then increases to 81.2% (x = 0.4). As mentioned above, Al substitution is prone to form a passive layer on the electrode surface in KOH electrolyte, which inevitably weakens the surface electrochemical catalytic activity and prevents the diffusion of hydrogen into or from the alloy bulk. Fortunately, it is reported that the addition of Mo to the alloy leads to the improvement of the electrocatalytic activity on the alloy surface [20]. Therefore, it is reasonable to assume that, with Al and Mo content addition of lower than a certain amount, the negative effect of Al is dominant and will cause a decrease in the HRD. However, when Al and Mo content exceed the critical content, the positive effect of Mo will become dominant and will give rise to increase of HRD. It present study, the critical content amount of Al and Mo addition is x = 0.2 from our work.

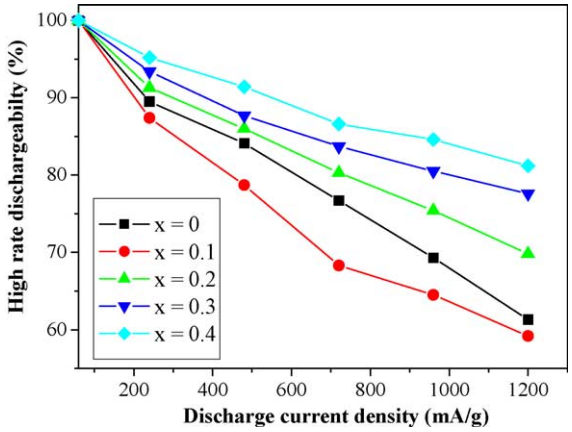

Fig. 7. High rate dischargeability of the $La_{0.7}Mg_{0.3}Ni_{3-x}$ $(Al_{0.5}Mo_{0.5})_x$ (x = 0, 0.1, 0.2, 0.3, 0.4) alloy electrodes at 298 K.

It is generally accepted that the HRD of metal hydride electrode is determined jointly by the exchange current density and the diffusion coefficient of hydrogen [28]. To examine the effect of the partial substitution of Al and Mo for Ni on the discharge kinetics, linear polarization is preformed on these alloy electrodes. Based on the measured linear polarization curves, values of exchange current density I_0 and polarization resistance R_p were calculated for the alloy electrodes and summarized in Table 4. Fig. 8 shows HRD and R_P as a function of I_0 for the hydrogen evolution reaction at the alloy electrodes. The HRD shows a linear re-

Table 4
Electrochemical kinetic parameter of $La_{0.7}Mg_{0.3}Ni_{3-x}(Al_{0.5}Mo_{0.5})_x$ (x = 0–0.4) alloy electrodes

Sample	Polarization resistance, R_p (mΩ)		Exchange current density, I_0 (mA/g)		Hydrogen diffusion coefficient, D ($\times 10^{-10}$ cm^2/s)	
	298 K	233 K	298 K	233 K	298 K	233 K
x = 0	102.42	363.60	224.38	55.15	12.3	1.3
x = 0.1	103.83	359.04	221.33	55.85	12.3	2.4
x = 0.2	94.24	353.54	243.85	56.72	12.7	2.9
x = 0.3	89.95	352.54	255.5	56.88	12.8	3.8
x = 0.4	88.83	349.65	258.71	57.35	13.1	4.9

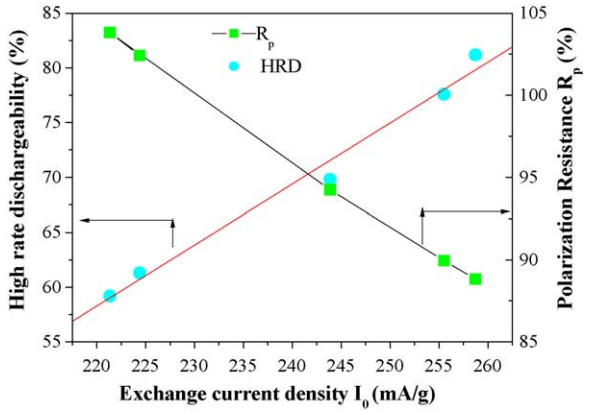

Fig. 8. High rate dischargeability and polarization resistance as a function of exchange current density for hydrogen evolution reaction at $La_{0.7}Mg_{0.3}Ni_{3-x}(Al_{0.5}Mo_{0.5})_x$ ($x = 0$–0.4) alloy electrodes.

lationship with the exchange density for the alloy electrodes. Moreover, we can find that the hydrogen diffusion coefficient D maintains almost unchanged (12.3–13.1 $\times 10^{-10}$ cm^2/s). Therefore, in the present study, the HRD is essentially controlled by the charge-transfer reaction of hydrogen on the surface at a discharge current density of 1200 mAh/g. In addition, it can be seen that the R_P decreases with increasing I_0 while the high rate dischargeability increases reversely, implying that the R_P value is closed related to the HRD.

3.6. Low temperature dischargeability (LTD)

Ni-MH battery is expected to be capable of working at temperature down to 233 K in some civil applications at very cold areas [29]. However, the discharge capacity of the negative electrode in nickel-metal hydride decreases drastically with decreasing temperature [30]. Sakai et al. [19] pointed out that the dischargeability of the negative electrodes at relative low temperature is mainly influenced by the hydrogen diffusion and charge-transfer process occurring at the metal electrolyte interface. The hydrogen D of hydrogen in the bulk is measured using the method described by Iwakura et al. [20]. The LTD, expressed as $LTD_{233}(\%) = C_{233}/C_{298} \times 100$ (where C_{233} and C_{298} are the discharge capacity at 233 and 298 K, respectively). The D and the I_0 of the $La_{0.7}Mg_{0.3}Ni_{3-x}(Al_{0.5}Mo_{0.5})_x$ ($x = 0$, 0.1, 0.2, 0.3, 0.4) alloy electrodes at 233 K are also tabulated in Table 4. It can found that both the I_0 and the D are smaller than that at 298 K. Moreover, we can find that the I_0 maintain almost unchanged (55.15–57.35 mA/g); whereas the D increases remarkably with increasing x, which implies that the hydrogen diffusion in alloy probably becomes the rate-determining factor for Low-temperature dischargeability at 233 K. Fig. 9 shows the LTD as a function of D in the alloy electrodes. It can be easily found that the D increases monotonically with increasing x in the alloys, and thus increases the LTD of the alloy electrodes.

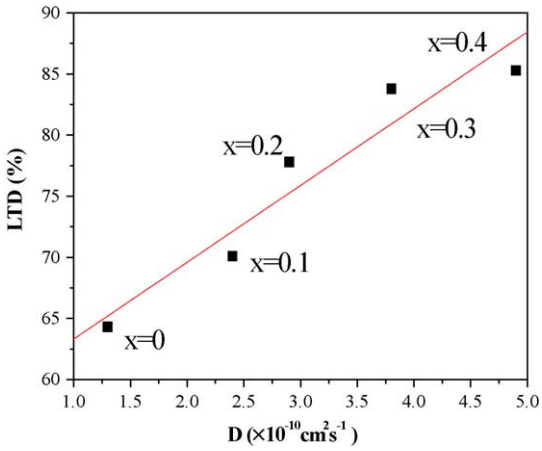

Fig. 9. The LTD as a function of D of the $La_{0.7}Mg_{0.3}Ni_{3-x}(Al_{0.5}Mo_{0.5})_x$ ($x = 0$, 0.1, 0.2, 0.3, 0.4) alloy electrodes at 233 K.

4. Conclusion

The structure and electrochemical properties of the $La_{0.7}Mg_{0.3}Ni_{3-x}(Al_{0.5}Mo_{0.5})_x$ ($x = 0$–0.4) hydrogen storage alloys have been investigated systematically. The Rietveld analysis results show that all these alloys consist mainly of a $La(La, Mg)_2Ni_9$ phase and a $LaNi_5$ phase. The P–C–T curves indicate that the hydrogen storage capacity first increases and then decreases with increasing x. The electrochemical measurements show that the maximum discharge capacity of the alloy electrode increases first from 343.3 ($x = 0$) to 377.6 mAh/g ($x = 0.3$) and then decreases to 350.4 mAh/g ($x = 0.4$). For the discharge current density of 1200 mA/g, the high rate HRD first decreases from 61.3% to 59.2% and then increases to 81.2%, which is consistent with the results of the exchange current density of the alloy electrodes. The hydrogen diffusion coefficient increases with increasing Al and Mo content, and thus increases the low temperature dischargeability of the alloy electrodes.

Acknowledgement

This work was financially supported by the National Natural Science Foundation of China (grant no.20171042).

References

[1] M. Latroche, A. Percheron-Guegan, J. Alloys Compd. 356 (2003) 461.
[2] J.J.G. Willems, K.H.J. Buschow, J. Less-Common Met. 13 (1987) 129.
[3] H.G. Pan, Y.F. Zhu, M.X. Gao, Q.D. Wang, J. Electrochem. Soc. 149 (2002) 829.
[4] T. Kohno, H. Yoshida, F. Kawashima, T. Inaba, I. Sakai, M. Yamamoto, M. Kanda, J. Alloys Compd. 311 (2000) 5.
[5] J.J.G. Willems, Philips J. Res. 39 (Suppl. 1) (1984) 1.
[6] J. Chen, N. Kuriyama, H.T. Takeshita, H. Tanaka, T. Sakai, M. Haruta, Electrochem. Solid-State Lett. 3 (6) (2000) 249.

[7] T. Sakai, I. Uehara, H. Iwakura, J. Alloys Compd. 293–295 (1999) 762.
[8] J.J. Reilly, G.D. Adzic, J.R. Johnson, T. Vogt, S. Mukerjee, J. McBreen, J. Alloys Compd. 293–295 (1999) 569.
[9] Y.F. Liu, H.G. pan, Y.F. Zhu, R. Li, Y.Q. Lei, Mater. Sci. Eng. A A372 (2004) 163.
[10] H. Oesterreicher, H. Bittner, J. Less-Common Met. 73 (1980) 339.
[11] K. Kadir, N. Nuriyama, T. Sakai, I. Uehara, L. Eriksson, J. Alloys Compd. 284 (1999) 145.
[12] K. Kadir, T. Sakai, I. Uahara, J. Alloys Compd. 287 (1999) 264.
[13] K. Kadir, T. Sakai, I. Uahara, J. Alloys Compd. 302 (2000) 112.
[14] J. Chen, H.T. Takeshita, H. Tanaka, N. Kuriyama, T. Sakai, J. Alloys Compd. 302 (2000) 304.
[15] T. Kohno, H. Yoshida, F. Kawashima, T. Inaba, I. Sakai, M. Yamamoto, M. Kanda, J. Alloys Compd. 311 (2000) L5.
[16] B. Liao, Y.Q. Lei, L.X. Chen, G.L. Lu, H.G. Pan, Q.D. Wang, J. Power Sources 129 (2004) 358.
[17] P.H. Notton, P. Hokkeling, J. Electrochem. Soc. 138 (1991) 1877.
[18] T. Sakai, H. Miyamura, N. Kuriyama, A. Kato, K. Oguro, H. Ishikawa, J. Less-Common Met. 159 (1990) 127.
[19] T. Sakai, H. Miyamura, N. Kuriyama, A. Kato, K. Oguro, H. Ishikawa, J. Electrochem. Soc. 137 (1990) 795.
[20] C. Iwakura, H. Senoh, K. Morimoto, Y. Hara, H. Inoue, Electrochemistry 70 (1) (2002) 2.
[21] M.T. Yeh, V.M. Beibutian, S.E. Hsu, J. Alloys Compd. 293–295 (1999) 721.
[22] C.J. Howard, J. Appl. Cryst. 15 (1982) 615.
[23] X.B. Zhang, Y.J. Chai, W.Y. Yin, M.S. Zhao, J. Solid State Chem. 177 (2004) 2373.
[24] X.B. Zhang, D.Z. Sun, W.Y. Yin, Y.J. Chai, M.S. Zhao, Electrochim. Acta, 50 (2005) 2911–2918.
[25] H. Oesterreicher, J. Clinton, H. Bittner, Mater. Res. Bull. 11 (1976) 1241.
[26] D.L. Sun, Y.Q. Lei, W.H. Liu, J.J. Jiang, J. Wu, Q.D. Wang, J. Alloys Compd. 231 (1995) 621.
[27] H.G. Pan, Y.F. Liu, M.X. Gao, Y.Q. Lei, Q.D. Wang, J. Electrochem. Soc. 150 (5) (2003) 565.
[28] T. Sakai, H. Miyamura, N. Kuriyama, A. Kato, K. Oguro, H. Ishikawa, J. Less-Common Met. 159 (1990) 127.
[29] T.B. Atwater, P.J. Cygan, F.C. Leung, J. Power Sources 91 (2000) 27.
[30] H. Senoh, Y. Hara, H. Inoue, C. Iwakura, Electrochim. Acta 46 (2001) 967.